Citation
Zhang, S. and Lyu, X. and Hurtado Torres, C. and Darwish, N. and Ciampi, S. 2022. Non-Ideal Cyclic Voltammetry of Redox Monolayers on Silicon Electrodes: Peak Splitting is Caused by Heterogeneous Photocurrents and Not by Molecular Disorder. Langmuir. 38 (2): pp. 743-750. http://doi.org/10.1021/acs.langmuir.1c02723

Non-ideal cyclic voltammetry of redox monolayers on silicon electrodes: peak splitting is caused by heterogeneous photocurrents and not by molecular disorder

*Song Zhang, Xin Lyu, Carlos Hurtado Torres, Nadim Darwish, Simone Ciampi**

School of Molecular and Life Sciences, Curtin University, Bentley, Western Australia 6102, Australia

ABSTRACT. Over the last three decades, research on redox-active monolayers has consolidated their importance as advanced functional material. For widespread monolayer systems, such as alkanethiols on gold, non-ideal multiple peaks in cyclic voltammetry are generally taken as indication of heterogeneous intermolecular interactions – namely disorder in the monolayer. Our findings show that, contrary to metals, peak multiplicity in silicon photoelectrodes is not diagnostic of heterogeneous intermolecular microenvironments, but is more likely caused by photocurrent being heterogeneous across the monolayer. This work is an important step towards understanding the cause of electrochemical non-idealities in semiconductor electrodes, so that these can be prevented and the redox behavior of molecular monolayers, as photocatalytic systems, optimized.

Introduction

Chemical reactions that are coupled to charge transfer events – the realm of redox chemistry – have wide-ranging ramifications across nature and are broadly exploited in technology.[1-2] The physical and chemical properties of the interface where a redox reaction takes place govern both its thermodynamics and kinetics.[3-5] Gaining control of the molecular features of electrode surfaces has therefore been pivotal in advancing our understanding of heterogeneous redox reactivity.[6] Prompted by the 1980 work of Sagiv on irreversible adsorption reactions of organic molecules on solids,[7] molecular self-assembly on solid electrodes remains one of the principal laboratory resources in the study of redox chemistry.[8-9] Redox reactivity can for instance be controlled by i) engineering changes to the density of surface redox molecules, hence to intermolecular interactions,[10-13] interfacial bonding[14] and surface conductivity,[15] ii) by controlling monolayer order,[16] and iii) by adjusting ion-pairing between redox entity and electrolyte ions.[17] Research on the latter – the engineering of ion-pair interactions – such as electrostatic interactions between surface ferrocenium molecules and soluble anions (e.g. $Fc + X^- \leftrightharpoons Fc^+–X^- + e^-$),[4, 17-20] is at the centre of the emerging electrochemistry sub-field of "electrolyte engineering". These interactions can be probed by dynamic electrochemical measurements – primarily cyclic voltammetry (CV)[21] – during the process of studying kinetics and thermodynamics of an electrode reaction.[22-25] Through a CV measurement the magnitude and degree of such interactions is often gauged by an analysis of the full-width-at-half-maximum (fwhm hereafter) of oxidation and reduction current peaks, of peak positions, and of peak-to-peak separation.[11, 16, 19] The common appearance of multiple waves is generally taken as indication of these interactions being highly heterogeneous due to different causes, being disorder one of the most frequent.

Herein we demonstrate that unlike for metallic electrodes (Figure 1a) in the technologically relevant case of semiconductor photoelectrodes it is not advisable to make inferences on the

heterogeneity of the redox environment, such as disorder and local differences in Fc^{+}–X^{-} vs Fc–Fc interactions,[17] based solely on the appearance of multiple CV waves. We show that in semiconductors the appearance of this non-ideal CV feature – multiple waves for a one-electron redox reaction – does not require molecular disorder across the monolayer, but is more likely caused by heterogeneous photocurrent across the surface (Figures 1b and 1c). This is important because while most of the research on interfacial redox reactivity still relies on alkanethiol chemistry and gold substrates,[26] the field is rapidly expanding towards silicon electrodes.[27] Silicon remains the technologically most relevant material,[28-32] and silicon surfaces that are functionalized with organic monolayers have applications ranging from sensing,[33-37] chemical catalysis,[38] microscopy,[39-40] molecular electronics,[41-43] and data storage.[9, 44-45]

All silicon electrodes used in this study were protected against major oxidation by an hydrosilylation procedure,[46] through which hydrogen terminated silicon was reacted with a symmetrical α,ω-diyne (1,8-nonadiyne **1**, Figure 1d).[47] The hydrosilylation of diyne **1** with an hydrogen-terminated silicon surface results in an exceedingly stable alkenyl linkage (Si–C=C–)[48] in an ordered monolayer (**M-1**).[49] The distal end of this monolayer is an acetylene function, which permits the attachment of an azide-tagged ferrocene molecule (**2**, Figure 1d) via a copper-(I) catalyzed alkyne–azide cycloaddition (CuAAC) reaction.[50-51] The electrode doping type and level (p- and n-type, highly and lowly doped, HD and LD hereafter), as well as the level of substrate illumination (or lack of it) during the CV measurements were adjusted so to demonstrate that multiple oxidation and reduction waves for surface confined redox units are not linked to poor solvation and/or monolayer disorder, but instead caused by heterogeneity in the substrate photocurrent.

Experimental section

Chemicals. Unless specified otherwise, all chemicals were of analytical grade and used as received. 1,8-Nonadiyne (**1**, Figure 1), 11-(ferrocenyl)undecanethiol (95%), H_2O_2 (aqueous hydrogen peroxide, 30% w/w), H_2SO_4 (sulfuric acid, 95–97%), NH_4F (aqueous ammonium fluoride, 40%), $(NH4)_2SO_3•H_2O$ (ammonium sulfite monohydrate, 92%), HCl (hydrochloric acid, 35–37%) were purchased from Sigma-Aldrich and used for cleaning, etching, and modifying silicon wafers. Redistilled DCM (dichloromethane), propan-2-ol and ethanol were utilized for substrate cleaning and monolayer-forming procedures. Milli-Q water (>18 MΩ cm) was used for substrate cleaning and modification and to prepare electrolytic solutions. Azidomethylferrocene (**2**, Figure 1d) was synthesized following a previously reported procedure.[47]

Silicon and gold crystals. Silicon wafers were of prime grade, single-side polished, prepared through the Czochralski process and purchased from Siltronix, S.A.S. (Archamps, France). Highly doped n-type Si(111), referred to as HD, was <111> ± 0.5° phosphorous-doped, with a thickness of 500 ± 25 μm and with a resistivity of 0.007–0.013 Ω cm. Lowly doped Si(111), referred to as LD, was <111> ± 0.5°, 7–13 Ω cm, phosphorous-doped, 500 ± 25 μm. Highly doped p-type Si(111) was <111> ± 0.5°, boron-doped, 500 ± 25 μm. Lowly doped n-type Si(100) was <100> ± 0.5°, phosphorous-doped, 500 ± 25 μm and 8–12 Ω cm. Gold single crystal electrodes (Au(111), 99.999%) were purchased from Goodfellow (Huntingdon, England), polished on one side to 1 μm or better, and flame-annealed prior to use.

Silicon surface modification. Prior to any chemical modification, samples were cut into squares of 1 × 1 cm, rinsed with DCM, propan-2-ol, and water. Samples were then immersed for at least 30 min in hot piranha solution (100 ºC, a 3:1 mixture (v/v) of concentrated sulphuric acid (95–97%) and hydrogen peroxide (30%)), rinsed with water and immediately transferred to a degassed (by means of bubbling argon gas for more than 30 minutes) aqueous 40% solution of NH_4F. This

etching solution contained a trace amount of ammonium sulphite (ca. 2 mg) added as oxygen scavenger. The silicon etching in the NH_4F solution for 9 min, rinsed with copious Milli-Q water and dichloromethane, then immediately reacted with 1,8-nonadiyne (which is degassed with nitrogen for 30min). The liquid sample of the α, ω-diyne (ca. 50 µl) was dropped on the hydrogen-terminated silicon surface and then irradiated under UV light for 2 hours under nitrogen atmosphere (Vilber, VL-215.M, $\lambda = 312$ nm, nominal power output of 30 W and set approximately 20 cm away from the silicon sample). The silicon substrates modified with monolayers of 1,8-nonadiyne were then rinsed three times with propan-2-ol and kept for 12 h in a reaction vial under DCM prior to the CuAAC surface modification step. The CuAAC reaction was performed as follow: to a reaction vial containing the alkyne-terminated substrate were added 5 mL of azidomethylferrocene solution (**2**, 0.5 mM in in a propan-2-ol and water mixture, 1:1, v/v), sodium ascorbate (100 mol % relative to the azide) and then copper (II) sulphate pentahydrate (20 mol % relative to the azide). The reaction was carried out at room temperature under dark, and quenched by decanting the liquid after 40 min (unless specified otherwise). The electrodes tethered with ferrocene molecules (**M-2**, Figure 1d) were immediately rinsed with copious amounts of propan-2-ol, water, 0.5 M aqueous HCl, water, propan-2-ol, DCM, blown dry under nitrogen and kept under DCM before analysis.

Gold surface modification. Au(111) crystals were annealed in a butane gas flame to yellow color and then quenched in DCM. The crystals were then transferred to an ethanolic 1.0 mM solution of 11-(ferrocenyl)undecanethiol, and rested in this monolayer-forming solution for 24 h. The modified electrodes were then rinsed with copious ethanol and immediately analyzed.

Electrochemical measurements. Cyclic voltammetry (CV) experiments were carried out with a CHI650D potentiostat (CH Instruments, Austin, Texas) using a three-electrode and single-

compartment polytetrafluoroethylene custom cell. The modified silicon substrate (**M-2**) or the Au(111) crystal coated with a self-assembled monolayer of 11-(ferrocenyl)undecanethiol served as the working electrode, a platinum mesh as the counter electrode, and a Ag/AgCl (3.0 M NaCl) electrode as the reference electrode. A circular Viton gasket defined the geometric area of the working electrode to 0.28 cm^2, and Ohmic contact between the back of the silicon sample and a copper plate was obtained by gently scribing the back of the electrode with emery paper before applying on it a small amount of the gallium−indium eutectic. Unless specified otherwise, the electrolyte was aqueous 1.0 M perchloric acid ($HClO_4$). All measurements were carried out in air at room temperature (22 ± 2°C) and under either dark or red light. The red light was a collimated deep red LED (660 nm, nominal power output 1050 mW, Thorlabs part M660L4 coupled to a SM1P25-A collimator adapter) illuminating the silicon electrode through the electrolyte. The collimator–sample distance was approximately 7 cm. The LED current was adjusted in six levels (LEDD1B, Thorlabs) to yield the following light intensities measured at the silicon surface: level 1, 1.0 mW cm^{-2}; level 2, 2.9 mW cm^{-2}; level 3, 4.7 mW cm^{-2}; level 4, 11.1 mW cm^{-2}; level 5, 24.1 mW cm^{-2}; level 6, 29.9 mW cm^{-2} (the illuminance was measured with a light meter from Amprobe, IC-LM-200 and the lx output was subsequently converted to mW cm^{-2} assuming 1 lx = 0.0024 mW cm^{-2}). Simulations of the voltammograms were performed in Wolfram Mathematica (Version 11) using a previously reported model.[52] All reported potentials are relative to the reference electrode. Surface coverages (Γ) of ferrocene molecules on silicon substrate were reported in mol cm^{-2} and calculated from the Faradaic charge taken as the background-subtracted integrated current from the anodic scan of the voltammograms.[53-54] Electrochemical impedance spectroscopy (EIS) data were collected between 10^5 Hz and 1 Hz, at an applied working electrode DC potential, E_{dc}, equal to −0.3 V and with an AC perturbation of 15 mV.

Atomic force microscopy. Current-potential curves (I–Vs) for the monolayer-modified silicon samples were performed using Park Atomic Force Microscopy (AFM) NX10 (Park Systems Corporation, Suwon, Korea), in conductive mode using solid platinum tips (12Pt300B, Rocky Mountain Nanotechnology, Holladay, UT) with a nominal resonance frequency of 9 kHz and a nominal spring constant of 0.8 N/m. All the AFM data were analyzed with the image processing software XEI 4.3.4 developed by Park System Corporation. The I–V traces were sampled at 100 separate locations. When comparing leakage current differences, we neglected traces that reached current saturation.

Water contact angle. Measurements of the sessile water contact angle were performed on a CAM 101 optical contact angle meter (KSV Instruments Ltd., Finland). Measurements were conducted on three independently prepared and analyzed samples of each doping level, with four separate spots measured on each sample. The reported value is the arithmetic average of the 12 measurements. Data were analyzed using the KSV CAM Pendant Drop Surface Tension software (3.81).

Results and discussion

The appearance of multiple CV waves when single-crystal metallic electrodes are derivatized with redox monolayers is a relatively common observation.[55] This non-ideal electrochemical behavior is caused by disorder and heterogeneity of the redox environment,[56] but as expected when dealing with a metal, these are not linked to any photoeffect (Figure S1, Supporting Information). Since peak multiplicity in gold manifests generally only for high surface densities of the redox molecule under study,[20, 24] before exploring the conditions necessary for the systematic appearance

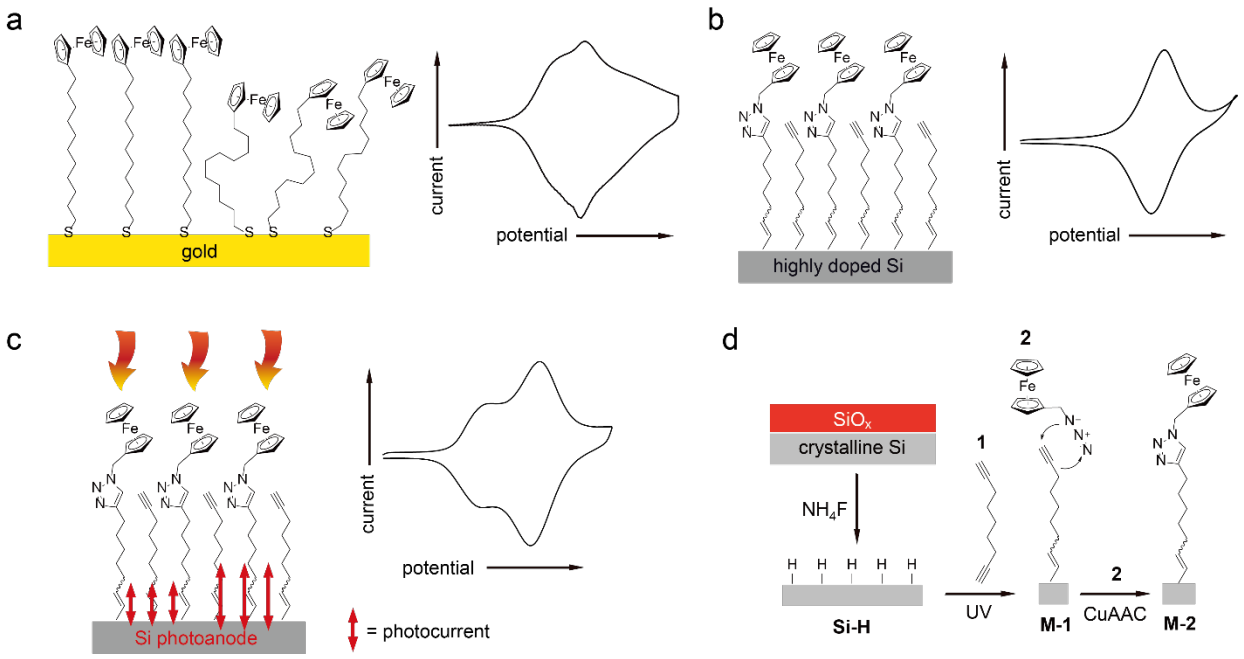

Figure 1. a) Schematic representation of an heterogeneous (ordered/disordered regions) monolayer-coated gold electrode, and (right) a typical cyclic voltammogram recorded on a single-crystal gold electrode modified with a monolayer of 11-ferrocenyl-1-undecanethiol (Au(111); 100 mV/s, 1.0 M $HClO_4$). b) Schematic depiction of a monolayer-coated silicon electrode, and near-ideal cyclic voltammetry (right) acquired on an highly doped silicon electrode coated with a ferrocene monolayer (0.007–0.013 Ω cm, p-type, Si(111); 100 mV/s, 1.0 M $HClO_4$). c) Schematic depiction of heterogeneous photocurrents across a silicon photoanode (1.0 mW cm^{-2}), and experimental evidence of peak-splitting in cyclic voltammetry (right) using a lowly doped silicon photocathode coated with a ferrocene monolayer (8–12 Ω cm, n-type, Si(111); 100 mV/s, 1.0 M $HClO_4$). d) Chemical strategy used for the passivation and derivatization of the hydrogen terminated silicon surface. The UV-assisted hydrosilylation of **1** on Si–H generates an alkyne-terminated surface (**M-1**), which is subsequently reacted with azidomethylferrocene (**2**) through a CuAAC reaction, yielding a redox-active monolayer (**M-2**).

of multiple redox waves in silicon we first tested to which degree the surface coverage of ferrocene units is reproducible and independent on the silicon crystal orientation and doping. As shown for example in Figure S2 (Supporting Information), the Faradaic charge obtained by integrating CV curves for **M-2** samples prepared on either Si(111) or Si(100) was not affected by doping level and type ($(1.99 \pm 0.84) \times 10^{-10}$ mol cm^{-2}, Si(111), LD, n-type; $(1.44 \pm 0.23) \times 10^{-10}$ mol cm^{-2} Si(100), LD, n-type; $(1.94 \pm 0.26) \times 10^{-10}$ mol cm^{-2}, Si(111), HD, p-type).

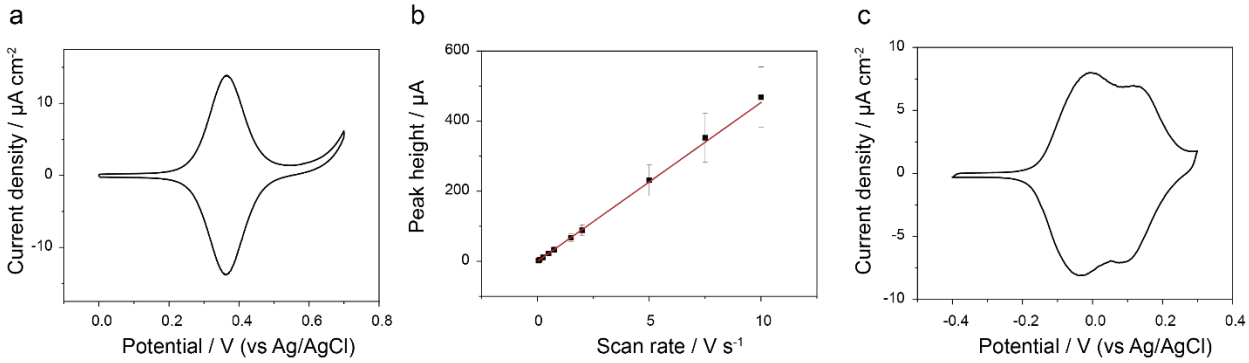

Figure 2. Doping level and type and ideality of the redox response. a) Representative and close-to-ideal cyclic voltammogram (CV) recorded for a **M-2** sample prepared on HD, p-type Si(111) (100 mV/s, 1.0 M $HClO_4$, dark, $\Gamma = 1.64 \times 10^{-10}$ mol cm^{-2}). b) Plot of current peak values (anodic waves) vs voltage scan rate (the error bars indicate the 95% confidence interval of the mean). c) A representative CV for a **M-2** monolayer grafted on a Si(111), n-type, LD photoanode, showing an evident non-ideal peak splitting (100 mV/s, 1.0 M $HClO_4$, electrode illuminated at a light intensity of 1.0 mW m^{-2}, $\Gamma = 1.95 \times 10^{-10}$ mol cm^{-2}).

Further, as can be seen from the data in Figure 2a, the current response from **M-2** samples upon cyclic bias ramping is of very good quality. Voltametric data presented in Figure 2a are obtained on p-type HD silicon operating in accumulation, so to prevent space-charge effects.[57] The CV waves had a fwhm of 115 ± 3 mV, and the presence and absence of illumination had no effect on the peak broadness (Figure S3, Supporting Information). The ideal fwhm expected from the Langmuir isotherm of a Nernstian process should be 90.6 mV, hence our experimental values are larger than ideal, which is not unusual,[58] and often explained as repulsive interactions between the electroactive species.[59] The peak current varied linearly with the voltage sweep rate, which confirms a surface-confined process (Figure 2b and Figure S4, Supporting Information). The exact same monolayer system (**M-2**) when prepared on n-type silicon of low doping (LD, Si(111)), showed however a far from ideal voltammetry (Figure 2c). As indicated above, surface coverages did not vary between substrates of different doping level and type, hence the **M-2** samples of Figure 2c are likely to have the same level of monolayer packing and order as the more ideal samples of Figure 2a. The only difference is that the system of Figure 2c is a photonanode

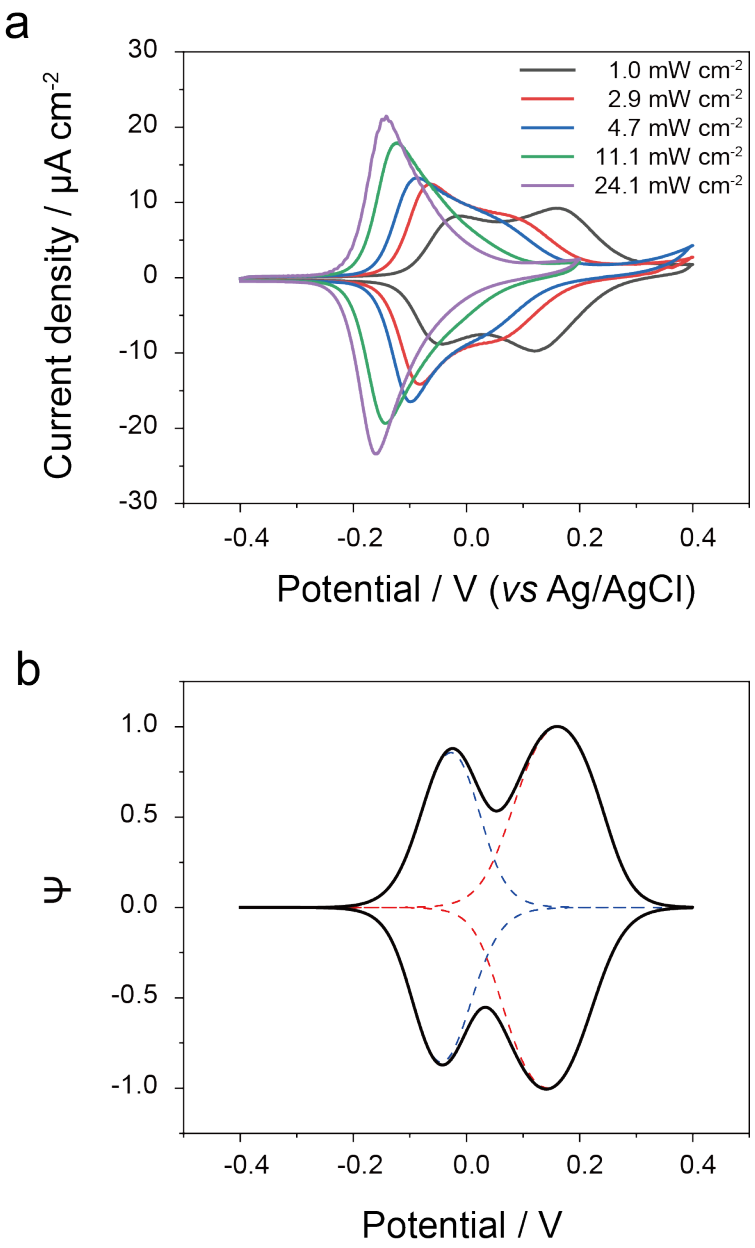

Figure 3. Peak multiplicity on Si(111) photoanodes: experiments and simulations. a) Progressive disappearance with increasing light intensity of the peak multiplicity characteristic of voltammograms recorded on silicon photoanodes. The electrodes are LD, n-type Si(111) crystals modified with a **M-2** monolayer. The level of electrode illumination is specified by labels to the CV traces. The electrolyte was 1.0 M $HClO_4$, and the scan rate 0.1 V/s. b) Simulation of the CV trace recorded at the lowest light intensity, demonstrating that the key feature of the experimental data, a 188 mV peak-to-peak separation, can be accounted for as surface domains with a 1,500 fold difference in photocurrent (larger photocurrent for the blue dashed trace). The self-interaction parameter, *G*, necessary to reproduce the experimental fwhm, is negative, indicating repulsive molecular interactions for ferrocenes in both domains (−1.4, red trace; −0.6, blue trace). Best fit parameters are 10 s^{-1} for the electron transfer rate constant, 1 μA for the dark leakage current, unity for the diode quality factor, and 0.5 for α.

(LD, n-type), requiring biasing of the silicon electrode–electrolyte interface into depletion to trigger the redox chemistry of ferrocene.[22, 59-60] This is because the ferrocene apparent formal potential lies anodic of the electrode's flat band potential,[57] and therefore electrode illumination is required to overcome the substantial kinetic barrier (Figure S5, Supporting Information). These photoanodes showed, as expected, a "contra-termodynamic" shift characteristic of a process mediated by valence-band holes (Figure S6, Supporting Information), but more interestingly they can display a very pronounced voltametric peak splitting (Figure 2c) at low light intensity. As stressed above, this double-peak feature, absent in HD p-type (Figure 2a), is unlikely related or caused by monolayer disorder, or by heterogeneous ion-pairing. As further proof of this last remark, the two peaks progressively merged into a single band upon a simple increase in light intensity (Figure 3a) despite illumination alone having no effect on the degree of monolayer order (Figure S1). Such effect is partially masked at larger scan rates (Figure S7, Supporting Information). To further reinforce on the order of the monolayer, electrochemical impedance data, acquired at a E_{dc} offset sufficiently different from the ferrocene apparent formal potential, showed that at low frequencies the phase angle approaches −90º, indicating that all samples are relatively free of imperfections (Figure S8, Supporting Information). We also remark that the appearance of the double-peak feature is still evident on samples of lower coverage (Figure S9, Supporting Information), where lateral interactions become even less likely. Further, no significant difference in water contact angle was found between **M-2** samples prepared on either n-type or p-type substrates (68° ± 4°, LD n-type; 67° ± 2°, HD p-type), suggesting substrate doping is unlikely to have an effect on monolayer structure.

As evident from the data in Figure 3a, two well resolved waves separated by approximately 190 mV at low light intensity (1.0 mW cm^{-2}), progressively merge into a single broad wave as the light

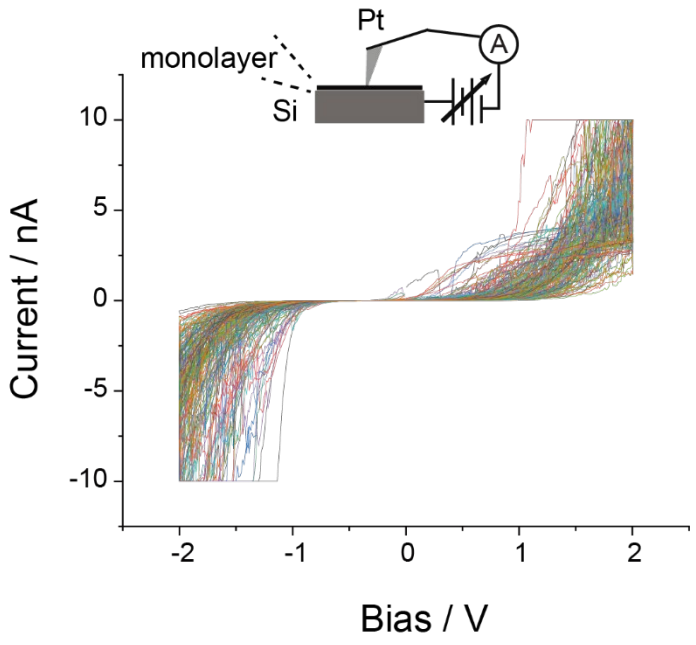

Figure 4. Lateral electrical heterogeneity. Current–potential (I–V) curves acquired by C-AFM on **M-1** samples (LD, n-type Si(111)) and measurement schematics of the platinum–monolayer–silicon junction. The bias routing is from the substrate to the AFM tip, so that the reverse current (leakage) of the junction appears in the positive quadrant (positive current, positive bias).

intensity was increased (up to ~24.1 mW cm^{-2}). Peak deconvolutions shown in Figure S10 (Supporting Information) indicate that the Faradaic charge of the individual contributions did not vary with illumination, while peak positions shifted progressively cathodic with increased irradiation. The origin of this shift is well known, and is the result of a logarithmic dependence of the electrode open circuit potential (E_{OCP}) on dark leakage current and photocurrent.[59] The *I–E* relationship for a cyclic voltammetry experiment, when interactions of the attached redox species (in the oxidized, O, and reduced, R, forms) are not negligible, was developed by Laviron assuming a Frumkin isotherm.[61-62] The Frumkin self-interaction parameter *G* was adjusted in our model (Figure 3b),[63-64] as changes to *G* account for the imbalance in the electrostatic push/pull, forcing the voltammetric wave to broaden or narrow when the activities of the reduced and oxidized species do not follow their surface concentrations.[23] Larger repulsive interactions (a more negative

G, see Figure 3b) are probably experienced by surface ferrocene units sensing a smaller photocurrent (more anodic E_{OCP}, vide infra). The *G* parameter is purely phenomenological and no attempt is made to describe the nature of these interactions. Whether these interactions are cause, effect, or not linked to the magnitude of the surface photocurrent is at present unclear.

We therefore hypothesize that the two CV bands clearly visible at low levels of illumination on Si(111) photoanodes relates to an heterogeneous electrode E_{OCP}, most likely the result of differences in local photocurrents (Figure 3b). Shifts in the experimental "macroscopic" E_{OCP} with changes to the light intensity are well documented for both photoanodes and photocathodes,[23, 60] but the possibility of a local heterogeneity of this shift within a given sample is generally neglected. Simulations where the photocurrent was varied by a factor close to 1,500 could reproduce the ca. 190 mV experimental peak-to-peak separation (Figure 3b). Surface defects introducing energy levels in the band gap are a possible cause of heterogeneous "wet" photocurrents, and such defects should manifest as a degree of heterogeneity in "dry" electrical leakage currents. That is, large local differences in the dark leakage current across the sample should parallel the appearance of CV peak multiplicity. On a photoanode, an increase in dark leakage (not necessarily an electrochemical process) causes a progressive anodic shift of E_{OCP}[23] (Figure S11, Supporting Information) and electrical mapping of dry junctions did support the existence of a significant difference in leakage across a given sample. Current–potential (I–V) data acquired by conductive atomic force microscopy (C-AFM), shown in Figure 4, highlight such heterogeneity in leakage current (which in turn affect the forward bias), with the largest experimental variation being ~400 folds at a bias of 0.6 V. I–Vs were sampled from 100 locations across the sample (Figure 4 and Figure S12, Supporting Information) and it is probable that at forward biases larger than 1.6 V the scatter in the current leakage is even larger, but as can be seen in Figure 4 above this bias several

traces are already beyond the range of the current amplifier. This current saturation is however not a serious shortcoming, as a comparison between electrical and electrochemical experiments is meaningful at a significantly lower bias. To select the sample bias at which a comparison between the "dry" leakage current, sampled at different microscopic locations, becomes valuable in attempting to explain the macroscopic "wet" CV response, we first assessed the "wet" flat-band potential, E_{FB}, of the electrode–electrolyte interface. E_{FB} was estimated from EIS Mott–Schottky (MS) measurements of capacitance vs sample bias. MS measurements shown in Figure S13 (Supporting Information) suggest a E_{FB} of ~ –0.57 V vs Ag/AgCl. Considering that the apparent formal potential of the Fc/Fc^+ couple in dark is ~0.35 V, there is therefore a ~ 0.92 V gap between the onset of accumulation and the apparent formal potential. In the electrical "dry" measurements (I–V) the magnitude of the leakage current scatter across a macroscopic sample (Figure 4) was therefore evaluated at a junction voltage of 0.92 V, being this the "dry" bias that best matches the 0.92 V "wet" gap described above (the flat-band of the silicon–platinum junction was estimated to be around 0 V, i.e. where the current generally starts its exponential rise). At this sampling point the largest difference in leakage was 204 folds, which is smaller than the 1000 folds difference in dark reverse current suggested by the model as required to account for the experimental CV peak separations if the photocurrent is unchanged (Figure S11, Supporting Information). It is therefore most likely that the experimental peak splitting is almost entirely caused by a heterogeneous photocurrent across the macroscopic monolayer system, as in fact changing the illumination intensity minimize the splitting (Figure 3). A dependency of photocurrent on the reverse dark leakage is not unprecedented,[65] and therefore the cause of photocurrent heterogeneity is probably rooted in the broad variability of the latter. Future measurements of lateral heterogeneity in the degree of Fermi-level pinning,[66-67] for instance by harvesting the latest developments in light-

addressed potentiometric sensors,[32, 36] could be used to advance our understanding of the silicon–electrolyte interface.

Conclusions

A complete and correct understanding of the factors governing how charges are transferred across a semiconductor interface underpins the design of devices whose function span from converting light into electricity, to sensing their environment. Among these factors a key one is the apparent formal potential of surface confined redox reactions. When the scientist and engineer require an analytical tool for such measurement, cyclic voltammetry still reigns supreme. Chemists, material scientists and engineers encountering non-ideal shapes and positions in voltammograms of electrodes modified with molecules are often inclined to reject these features as disorder in the adsorbate layer. Here we have shown that at monolayer-modified crystalline silicon electrodes multiple voltammetric waves are not necessarily diagnostic of molecular disorder, but instead caused by heterogeneous leakage (reverse bias) currents across the monolayer system. The leakage heterogeneity, probed by conductive AFM, causes photocurrents to vary across the sample, hence brings about changes to the local E_{OCP}, which finally manifest as multiple redox bands.

ASSOCIATED CONTENT

Supporting Information. Additional AFM, cyclic voltammetry, EIS Mott–Schottky plots. This material is available free of charge via the Internet at http://pubs.acs.org.

AUTHOR INFORMATION

Corresponding Author

Simone Ciampi − School of Molecular and Life Sciences, Curtin University, Bentley, Western Australia 6102, Australia; orcid.org/0000-0002-8272-8454; Email: simone.ciampi@curtin.edu.au

Authors

Song Zhang – School of Molecular and Life Sciences, Curtin University, Bentley, Western Australia 6102, Australia; orcid.org/0000-0002-3387-4957

Xin Lyu – School of Molecular and Life Sciences, Curtin University, Bentley, Western Australia 6102, Australia; orcid.org/0000-0002-6506-0392

Carlos Hurtado Torres – School of Molecular and Life Sciences, Curtin University, Bentley, Western Australia 6102, Australia

Nadim Darwish – School of Molecular and Life Sciences, Curtin University, Bentley, Western Australia 6102, Australia; orcid.org/0000-0002-6565-1723

Notes

The authors declare no competing financial interest.

ACKNOWLEDGMENTS

The authors acknowledge support from the Australian Research Council (DP190100735 and FT190100148).

References

(1) Blanco, D. E.; Modestino, M. A., Organic Electrosynthesis for Sustainable Chemical Manufacturing. *Trends Chem.* **2019,** *1*, 8-10.
(2) Lisdat, F., Coupling biology to electrochemistry—future trends and needs. *J. Solid State Electrochem.* **2020,** *24*, 2125-2127.

(3) Gileadi, E., *Electrode Kinetics for Chemists, Chemical Engineers and Materials Scientists*. Wiley-VCH Verlag GmbH: New York, 1993; p 597.
(4) Rowe, G. K.; Creager, S. E., Redox and ion-pairing thermodynamics in self-assembled monolayers. *Langmuir* **1991,** *7*, 2307-2312.
(5) Vogel, Y. B.; Evans, C.; Belotti, M.; Xu, L.; Russell, I.; Yu, L.-J.; Fung, A.; Hill, N.; Darwish, N.; Gonçales, V.; Coote, M. L.; Iyer, S.; Ciampi, S., The Corona of a Surface Bubble Promotes Electrochemical Reactions. *Nat. Commun.* **2020,** *11*, 6323.
(6) Eckermann, A. L.; Feld, D. J.; Shaw, J. A.; Meade, T. J., Electrochemistry of redox-active self-assembled monolayers. *Coord. Chem. Rev.* **2010,** *254*, 1769-1802.
(7) Sagiv, J., Organized Monolayers by Adsorption. 1. Formation and Structure of Oleophobic Mixed Monolayers on Solid Surfaces. *J. Am. Chem. Soc.* **1980,** *102*, 92–98.
(8) Gooding, J. J.; Ciampi, S., The Molecular Level Modification of Surfaces: From Self-Assembled Monolayers to Complex Molecular Assemblies. *Chem. Soc. Rev.* **2011,** *40*, 2704-2718.
(9) Fabre, B., Functionalization of Oxide-Free Silicon Surfaces with Redox-Active Assemblies. *Chem. Rev.* **2016,** *116*, 4808–4849.
(10) Ciampi, S.; Choudhury, M. H.; Ahmad, S. A. B. A.; Darwish, N.; Brun, A. L.; Gooding, J. J., The Impact of Surface Coverage on the Kinetics of Electron Transfer through Redox Monolayers on a Silicon Electrode Surface. *Electrochim. Acta* **2015,** *186*, 216-222.
(11) Gonzalez, J.; Sequí, J.-A., Kinetic Implications of the Presence of Intermolecular Interactions in the Response of Binary Self-Assembled Electroactive Monolayers. *ACS Omega* **2018,** *3*, 1276-1292.
(12) Gonzalez, J.; Sequí-Castellano, J. A., Electrochemical determination of kinetic parameters of surface confined redox probes in presence of intermolecular interactions by means of Cyclic Voltammetry. Application to TEMPO monolayers in gold and platinum electrodes. *Electrochim. Acta* **2021,** *365*, 137331.
(13) Nerngchamnong, N.; Thompson, D.; Cao, L.; Yuan, L.; Jiang, L.; Roemer, M.; Nijhuis, C. A., Nonideal Electrochemical Behavior of Ferrocenyl–Alkanethiolate SAMs Maps the Microenvironment of the Redox Unit. *J. Phys. Chem. C* **2015,** *119*, 21978-21991.
(14) Dief, E. M.; Darwish, N., Ultrasonic Generation of Thiyl Radicals: A General Method of Rapidly Connecting Molecules to a Range of Electrodes for Electrochemical and Molecular Electronics Applications. *ACS Sens.* **2021,** *6*, 573–580.
(15) Zhang, S.; Ferrie, S.; Peiris, C. R.; Lyu, X.; Vogel, Y. B.; Darwish, N.; Ciampi, S., Common Background Signals in Voltammograms of Crystalline Silicon Electrodes are Reversible Silica–Silicon Redox Chemistry at Highly Conductive Surface Sites. *J. Am. Chem. Soc.* **2021,** *143*, 1267–1272.
(16) Laborda, E.; González, J.; Molina, A., Analytical Theory for Ion Transfer–Electron Transfer Coupled Reactions at Redox Layer–Modified/Thick Film–Modified Electrodes. *Curr. Opin. Electrochem.* **2020,** *19*, 78–87.
(17) Wong, R. A.; Yokota, Y.; Wakisaka, M.; Inukai, J.; Kim, Y., Probing consequences of anion-dictated electrochemistry on the electrode/monolayer/electrolyte interfacial properties. *Nat. Commun.* **2020,** *11*, 4194.
(18) Yokota, Y.; Yamada, T.; Kawai, M., Ion-Pair Formation between Ferrocene-Terminated Self-Assembled Monolayers and Counteranions Studied by Force Measurements. *J. Phys. Chem. C* **2011,** *115*, 6775-6781.

(19) Zhang, L.; Vogel, Y. B.; Noble, B. B.; Goncales, V. R.; Darwish, N.; Brun, A. L.; Gooding, J. J.; Wallace, G. G.; Coote, M. L.; Ciampi, S., TEMPO Monolayers on Si(100) Electrodes: Electrostatic Effects by the Electrolyte and Semiconductor Space-Charge on the Electroactivity of a Persistent Radical. *J. Am. Chem. Soc.* **2016,** *138*, 9611–9619.
(20) Darwish, N.; Eggers, P. K.; Ciampi, S.; Tong, Y.; Ye, S.; Paddon-Row, M. N.; Gooding, J. J., Probing the Effect of the Solution Environment around Redox-Active Moieties Using Rigid Anthraquinone Terminated Molecular Rulers. *J. Am. Chem. Soc.* **2012,** *134*, 18401-18409.
(21) Heinze, J., Cyclic Voltammetry—"Electrochemical Spectroscopy". New Analytical Methods (25). *Angew. Chem. Int. Ed.* **1984,** *23*, 831–847.
(22) Santangelo, P. G.; Miskelly, G. M.; Lewis, N. S., Cyclic Voltammetry at Semiconductor Photoelectrodes. 1. Ideal Surface-Attached Redox Couples with Ideal Semiconductor Behavior. *J. Phys. Chem.* **1988,** *92*, 6359-6367.
(23) Vogel, Y. B.; Zhang, L.; Darwish, N.; Gonçales, V. R.; Le Brun, A.; Gooding, J. J.; Molina, A.; Wallace, G. G.; Coote, M. L.; Gonzalez, J.; Ciampi, S., Reproducible flaws unveil electrostatic aspects of semiconductor electrochemistry. *Nat. Commun.* **2017,** *8*, 2066.
(24) Eggers, P. K.; Darwish, N.; Paddon-Row, M. N.; Gooding, J. J., Surface-Bound Molecular Rulers for Probing the Electrical Double Layer. *J. Am. Chem. Soc.* **2012,** *134*, 7539–7544.
(25) Zhang, S.; Ferrie, S.; Lyu, X.; Xia, Y.; Darwish, N.; Wang, Z.; Ciampi, S., Absence of a Relationship between Surface Conductivity and Electrochemical Rates: Redox-Active Monolayers on Si(211), Si(111), and Si(110). *J. Phys. Chem. C* **2021,** *125*, 18197-18203.
(26) Vericat, C.; Vela, M. E.; Benitez, G.; Carro, P.; Salvarezza, R. C., Self-Assembled Monolayers of Thiols and Dithiols on Gold: New Challenges for a Well-Known System. *Chem. Soc. Rev.* **2010,** *39*, 1805–1834.
(27) Fabre, B., Functionalization of Oxide-Free Silicon Surfaces with Redox-Active Assemblies. *Chem. Rev.* **2016,** *116*, 4808-4849.
(28) Landman, U.; Barnett, R. N.; Scherbakov, A. G.; Avouris, P., Metal-Semiconductor Nanocontacts: Silicon Nanowires. *Phys. Rev. Lett.* **2000,** *85*, 1958–1961.
(29) Lapano, J.; Brahlek, M.; Zhang, L.; Roth, J.; Pogrebnyakov, A.; Engel-Herbert, R., Scaling growth rates for perovskite oxide virtual substrates on silicon. *Nat. Commun.* **2019,** *10*, 2464.
(30) Zhang, H.; Liu, H.; Wei, K.; Kurakevych, O. O.; Le Godec, Y.; Liu, Z.; Martin, J.; Guerrette, M.; Nolas, G. S.; Strobel, T. A., BC8 Silicon (Si-III) is a Narrow-Gap Semiconductor. *Phys. Rev. Lett.* **2017,** *118*, 146601.
(31) Schmehl, A.; Vaithyanathan, V.; Herrnberger, A.; Thiel, S.; Richter, C.; Liberati, M.; Heeg, T.; Rockerath, M.; Kourkoutis, L. F.; Muhlbauer, S.; Boni, P.; Muller, D. A.; Barash, Y.; Schubert, J.; Idzerda, Y.; Mannhart, J.; Schlom, D. G., Epitaxial Integration of the Highly Spin-Polarized Ferromagnetic Semiconductor EuO with Silicon and GaN. *Nat. Mater.* **2007,** *6*, 882–887.
(32) Wang, J.; Yang, Z.; Chen, W.; Du, L.; Jiao, B.; Krause, S.; Wang, P.; Wei, Q.; Zhang, D.-W.; Wu, C., Modulated Light-Activated Electrochemistry at Silicon Functionalized with Metal-Organic Frameworks Towards Addressable DNA Chips. *Biosens. Bioelectron.* **2019,** *146*, 111750.
(33) Qin, G.; Santos, C.; Zhang, W.; Li, Y.; Kumar, A.; Erasquin, U. J.; Liu, K.; Muradov, P.; Trautner, B. W.; Cai, C., Biofunctionalization on Alkylated Silicon Substrate Surfaces via "Click" Chemistry. *J. Am. Chem. Soc.* **2010,** *132*, 16432–16441.

(34) Juan-Colás, J.; Parkin, A.; Dunn, K. E.; Scullion, M. G.; Krauss, T. F.; Johnson, S. D., The electrophotonic silicon biosensor. *Nat. Commun.* **2016,** *7*, 12769.
(35) Terrero Rodríguez, I. M.; Borrill, A. J.; Schaffer, K. J.; Hernandez, J. B.; O'Neil, G. D., Light-Addressable Electrochemical Sensing with Electrodeposited n-Silicon/Gold Nanoparticle Schottky Junctions. *Anal. Chem.* **2020,** *92*, 11444-11452.
(36) Chen, L.; Zhou, Y.; Jiang, S.; Kunze, J.; Schmuki, P.; Krause, S., High resolution LAPS and SPIM. *Electrochem. Commun.* **2010,** *12*, 758-760
(37) Wang, J.; Zhou, Y.; Watkinson, M.; Gautrot, J.; Krause, S., High-sensitivity light-addressable potentiometric sensors using silicon on sapphire functionalized with self-assembled organic monolayers. *Sens. Actuators, B* **2015,** *209*, 230-236.
(38) Pekarek, R. T.; Kearney, K.; Simon, B. M.; Ertekin, E.; Rockett, A. A.; Rose, M. J., Identifying Charge Transfer Mechanisms across Semiconductor Heterostructures via Surface Dipole Modulation and Multiscale Modeling. *J. Am. Chem. Soc.* **2018,** *140*, 13223–13232.
(39) Vogel, Y. B.; Darwish, N.; Ciampi, S., Spatiotemporal Control of Electrochemiluminescence Guided by a Visible Light Stimulus. *Cell Rep. Phys. Sci.* **2020,** *1*, 100107.
(40) Ciampi, S.; James, M.; Le Saux, G.; Gaus, K.; Justin Gooding, J., Electrochemical "Switching" of Si(100) Modular Assemblies. *J. Am. Chem. Soc.* **2012,** *134*, 844–847.
(41) Ciampi, S.; Gooding, J. J., Direct Electrochemistry of Cytochrome c at Modified Si(100) Electrodes. *Chem. Eur. J.* **2010,** *16*, 5961–5968.
(42) Chen, X.; Park, Y. J.; Kang, M.; Kang, S.-K.; Koo, J.; Shinde, S. M.; Shin, J.; Jeon, S.; Park, G.; Yan, Y.; MacEwan, M. R.; Ray, W. Z.; Lee, K.-M.; Rogers, J. A.; Ahn, J.-H., CVD-grown monolayer MoS2 in bioabsorbable electronics and biosensors. *Nat. Commun.* **2018,** *9*, 1690.
(43) Aragonès, A. C.; Darwish, N.; Ciampi, S.; Sanz, F.; Gooding, J. J.; Díez-Pérez, I., Single-Molecule Electrical Contacts on Silicon Electrodes under Ambient Conditions. *Nat. Commun.* **2017,** *8*, 15056.
(44) Fabre, B., Ferrocene-Terminated Monolayers Covalently Bound to Hydrogen-Terminated Silicon Surfaces. Toward the Development of Charge Storage and Communication Devices. *Acc. Chem. Res.* **2010,** *43*, 1509-1518.
(45) Fabre, B.; Pujari, S. P.; Scheres, L.; Zuilhof, H., Micropatterned Ferrocenyl Monolayers Covalently Bound to Hydrogen-Terminated Silicon Surfaces: Effects of Pattern Size on the Cyclic Voltammetry and Capacitance Characteristics. *Langmuir* **2014,** *30*, 7235–7243.
(46) Linford, M. R.; Chidsey, C. E. D., Alkyl monolayers covalently bonded to silicon surfaces. *J. Am. Chem. Soc.* **1993,** *115*, 12631-12632.
(47) Ciampi, S.; Böcking, T.; Kilian, K. A.; James, M.; Harper, J. B.; Gooding, J. J., Functionalization of Acetylene-Terminated Monolayers on Si(100) Surfaces: A Click Chemistry Approach. *Langmuir* **2007,** *23*, 9320–9329.
(48) Ciampi, S.; Eggers, P. K.; Le Saux, G.; James, M.; Harper, J. B.; Gooding, J. J., Silicon (100) Electrodes Resistant to Oxidation in Aqueous Solutions: An Unexpected Benefit of Surface Acetylene Moieties. *Langmuir* **2009,** *25*, 2530-2539.
(49) James, M.; Darwish, T. A.; Ciampi, S.; Sylvester, S. O.; Zhang, Z.; Ng, A.; Gooding, J. J.; Hanley, T. L., Nanoscale Condensation of Water on Self-Assembled Monolayers. *Soft Matter* **2011,** *7*, 5309-5318.

(50) Glaser, T.; Meinecke, J.; Länger, C.; Heep, J.; Koert, U.; Dürr, M., Solution-Based Alkyne–Azide Coupling on Functionalized Si(001) Prepared under UHV Conditions. *J. Phys. Chem. C* **2021,** *125*, 4021-4026.
(51) Wu, F.; Zhang, D.-W.; Wang, J.; Watkinson, M.; Krause, S., Copper Contamination of Self-Assembled Organic Monolayer Modified Silicon Surfaces Following a "Click" Reaction Characterized with LAPS and SPIM. *Langmuir* **2017,** *33*, 3170-3177.
(52) Vogel, Y. B.; Zhang, L.; Darwish, N.; Gonçales, V. R.; Le Brun, A.; Gooding, J. J.; Molina, A.; Wallace, G. G.; Coote, M. L.; Gonzalez, J.; Ciampi, S., Reproducible flaws unveil electrostatic aspects of semiconductor electrochemistry. *Nature Communications* **2017,** *8*, 2066.
(53) Laviron, E., Surface linear potential sweep voltammetry: Equation of the peaks for a reversible reaction when interactions between the adsorbed molecules are taken into account. *J. Electroanal. Chem. Interf. Electrochem.* **1974,** *52*, 395–402.
(54) Laviron, E., The use of linear potential sweep voltammetry and of a.c. voltammetry for the study of the surface electrochemical reaction of strongly adsorbed systems and of redox modified electrodes. *J. Electroanal. Chem.* **1979,** *100*, 263–270.
(55) Wong, R. A.; Yokota, Y.; Wakisaka, M.; Inukai, J.; Kim, Y., Probing consequences of anion-dictated electrochemistry on the electrode/monolayer/electrolyte interfacial properties. *Nature Communications* **2020,** *11*, 4194.
(56) Rudnev, A. V.; Yoshida, K.; Wandlowski, T., Electrochemical characterization of self-assembled ferrocene-terminated alkanethiol monolayers on low-index gold single crystal electrodes. *Electrochim Acta.* **2013,** *87*, 770-778.
(57) Choudhury, M. H.; Ciampi, S.; Yang, Y.; Tavallaie, R.; Zhu, Y.; Zarei, L.; Gonçales, V. R.; Gooding, J. J., Connecting Electrodes with Light: One Wire, Many Electrodes. *Chem. Sci.* **2015,** *6*, 6769-6776.
(58) Paxton, W. F.; Kleinman, S. L.; Basuray, A. N.; Stoddart, J. F.; Van Duyne, R. P., Surface-Enhanced Raman Spectroelectrochemistry of TTF-Modified Self-Assembled Monolayers. *J. Phys. Chem. Lett.* **2011,** *2*, 1145-1149.
(59) Vogel, Y. B.; Molina, A.; Gonzalez, J.; Ciampi, S., Quantitative Analysis of Cyclic Voltammetry of Redox Monolayers Adsorbed on Semiconductors: Isolating Electrode Kinetics, Lateral Interactions, and Diode Currents. *Anal. Chem.* **2019,** *91*, 5929-5937.
(60) Yang, Y.; Ciampi, S.; Choudhury, M. H.; Gooding, J. J., Light Activated Electrochemistry: Light Intensity and pH Dependence on Electrochemical Performance of Anthraquinone Derivatized Silicon. *J. Phys. Chem. C* **2016,** *120*, 2874-2882.
(61) Laviron, E., General Expression of the Linear Potential Sweep Voltammogram in the Case of Diffusionless Electrochemical Systems. *J. Electroanal. Chem. Interfacial Electrochem.* **1979,** *101*, 19-28.
(62) Laviron, E.; Roullier, L., General Expression of the Linear Potential Sweep Voltammogram for a Surface Redox Reaction with Interactions between the Adsorbed Molecules: Applications to Modified Electrodes. *J. Electroanal. Chem. Interfacial Electrochem.* **1980,** *115*, 65-74.
(63) Laviron, E., Surface linear potential sweep voltammetry: Equation of the peaks for a reversible reaction when interactions between the adsorbed molecules are taken into account. *J. Electroanal. Chem. Interf. Electrochem.* **1974,** *52*, 395-402.
(64) Laviron, E.; Roullier, L., General expression of the linear potential sweep voltammogram for a surface redox reaction with interactions between the adsorbed molecules. Applications to modified electrodes. *J. Electroanal. Chem. Interf. Electrochem.* **1980,** *115*, 65-74.

(65) Brenneis, A.; Overbeck, J.; Treu, J.; Hertenberger, S.; Morkötter, S.; Döblinger, M.; Finley, J. J.; Abstreiter, G.; Koblmüller, G.; Holleitner, A. W., Photocurrents in a Single InAs Nanowire/Silicon Heterojunction. *ACS Nano* **2015,** *9*, 9849-9858.
(66) Bard, A. J.; Bocarsly, A. B.; Fan, F. R. F.; Walton, E. G.; Wrighton, M. S., The concept of Fermi level pinning at semiconductor/liquid junctions. Consequences for energy conversion efficiency and selection of useful solution redox couples in solar devices. *J. Am. Chem. Soc.* **1980,** *102*, 3671-3677.
(67) Chazalviel, J. N.; Truong, T. B., Experimental study of the n-silicon/acetonitrile interface: Fermi level pinning and surface states investigation. *J. Am. Chem. Soc.* **1981,** *103*, 7447-7451.

Electrical origin of electrochemical non-idealities